Controls on upper ocean salinity variability in the eastern subpolar North Atlantic during 1992–2017

Ali H. Siddiqui[1], **Thomas W. N. Haine**[1], **An T. Nguyen**[2], **Martha W. Buckley**[3]

[1]Department of Earth and Planetary Sciences, Johns Hopkins University, Baltimore, MD, USA
[2]Oden Institute for Computational Engineering and Sciences, University of Texas at Austin, Austin, TX, USA
[3]Atmospheric, Oceanic and Earth Sciences, George Mason University, Fairfax, VA, USA

Key Points:

- Two fresh anomalies observed in the eastern subpolar North Atlantic upper ocean during 1992–2017 share similar spatial characteristics.
- Salt budget analysis shows the 2012–2016 fresh anomaly in the upper 1000 m occurs due to transport of anomalous salinity by mean currents.
- In contrast, the fresh anomaly in the 1990s is due to anomalous circulation of the mean salinity field.

Corresponding author: Ali H. Siddiqui, asiddi24@jhu.edu

Abstract

The upper ocean salinity in the eastern subpolar North Atlantic undergoes decadal fluctuations. A large fresh anomaly event occurred during 2012–2016. Using the ECCOv4r4 state estimate, we diagnose and compare mechanisms of this low salinity event with those of the 1990s fresh anomaly event. To avoid issues related to the choice of reference salinity values in the freshwater budget, we perform a salt mass content budget analysis of the eastern subpolar North Atlantic. It shows that the recent low salt content anomaly occurs due to the circulation of anomalous salinity by mean currents entering the eastern subpolar basin from its western boundary via the North Atlantic Current. This is in contrast to the early 1990s, when the dominant mechanism governing the low salt content anomaly was the transport of the mean salinity field by anomalous currents.

Plain Language Summary

On decadal time scales, the eastern subpolar North Atlantic shifts between a salty and fresh upper ocean. Between 2012 and 2016, there was a large event which freshened this region more than at any other time in over a century. A similar event occurred in the early 1990s, but with a smaller magnitude. We use a numerical model of the ocean to figure out why these events occurred. Our study shows that there were two different mechanisms at play. The recent event occurred because a lot of fresh water came in from the west by the mean currents. The 1990s event occurred because ocean currents shifted and brought fresh water from outside the region.

1 Introduction

Large scale low salinity events occur in the eastern subpolar North Atlantic Ocean (ESNA) on decadal time scales. Based on observations, the subpolar North Atlantic has been undergoing such decadal salinity changes since at least the early 20th century (Sundby & Drinkwater, 2007; Dickson et al., 1988; Dooley et al., 1984; R. Zhang & Vallis, 2006; Dickson et al., 1988; Belkin et al., 1998; Belkin, 2004). During the 1992–2017 period, there were two fresh anomaly events in the ESNA reaching maximum freshwater accumulation in 1995 and 2016 respectively.

We highlight previous discussion in the literature on mechanisms that control the salinity in the ESNA. These include changes in the strength and size of the subpolar gyre (SPG), local atmospheric forcing in the ESNA (Fox et al., 2022; Holliday et al., 2020), and advection of salt anomalies from the Arctic or the subtropics (J. Zhang et al., 2021; Yeager et al., 2012; Häkkinen et al., 2011; Thierry et al., 2008; Sundby & Drinkwater, 2007; Holliday, 2003).

The strength and size of the subpolar gyre has been hypothesized to play an important role in setting salinity variability in the ESNA (Holliday, 2003; Hátún et al., 2005; Häkkinen & Rhines, 2004; Sarafanov et al., 2008; Yeager et al., 2012; Häkkinen et al., 2011; Thierry et al., 2008), especially in the context of the warming and salinification that occurred in the mid 1990s to 2000s. The expansion of the SPG reduces the contribution of salty subtropical waters to the ESNA, reducing the salinity; in 1994 and 2016 sea surface height (SSH) contours show an expanded subpolar gyre and fresh anomalies in the ESNA (Fig. 1). In contrast, the contraction of the SPG allows more subtropical waters into the ESNA, increasing salinity; in 2008 the subpolar gyre is contracted, as SSH contours retreat westward, and the ESNA is saltier (Fig. 1).

Subsequent studies have refined diagnostics for studying the relationship between the subpolar gyre strength and ESNA salinity; Tesdal et al. (2018) analyze a density-based gyre index, which is a proxy for the baroclinic strength of the gyre (Koul et al., 2020). Foukal and Lozier (2017, 2018) suggest that the salinity in the ESNA is strongly

influenced by the intergyre transport, which is modulated by the Atlantic meridional overturning circulation (AMOC). Koul et al. (2020) perform Lagrangian tracking experiments based on multiple definitions of the SPG strength during 1993–2016 and conclude that the majority of virtual floats reaching ESNA originate from subtropical waters. However, contributions from subpolar-sourced waters increase five-fold during an expanded state of the SPG (1988–1994 and 2012–2016). Backward particle release experiments in the upper 200 m ESNA conducted by Haine et al. (2023) reach similar conclusions about the contribution of subpolar-sourced waters compared to subtropical waters.

Another method to diagnose mechanisms controlling temperature and salinity variability is by performing budget calculations. To address the decadal SST variability in the subpolar North Atlantic, Piecuch et al. (2017) calculated the heat budget for 46°–65°N and concluded that the warming in the late 1990s and subsequent cooling since 2008 are primarily driven by oceanic advective heat transport convergence. The anomalous convergence is dominated by anomalies across the southern boundary (46°N). Similar studies by Oldenburg et al. (2018) and Tesdal and Haine (2020) reach the same conclusion on the dominance of the southern boundary advection in setting subpolar North Atlantic heat and freshwater variability. Similarly, Sanders et al. (2022) investigate the 2015 anomalous cooling in the eastern and central subpolar region (defined over 50–20°W, 43–63°N) using a mixed layer heat budget. They observe that surface heat loss initiates and drives the cooling, with advection sustaining the anomaly in the region (as expected from Tesdal & Abernathey, 2021). They also emphasize the role of vertical diffusion across the base of the mixed layer in the re-emergence of the anomaly during summer of 2014.

Bryden et al. (2020) observed that there has been a mean increase of 0.12 ± 0.04 Sv in Atlantic freshwater transport (relative to a reference salinity of 35.17 psu) at 26°N after 2010 compared to before 2009. This increase is about 10% of the 2004–2009 average freshwater transport. They propose that the rate of freshwater content gain of 0.062 ± 0.013 Sv over the eastern subpolar gyre during 2014–16 relative to 2007–09 is primarily due to the reduction of the AMOC by 2.5 Sv after 2009.

Changes in the Labrador Sea, mediated by changes in atmospheric forcing, also have been implicated for freshwater changes in the ESNA. Holliday et al. (2020) suggest that the primary mechanism of freshwater gain for the 2012–2017 freshening event in the Icelandic basin is the rerouting of Arctic-sourced Labrador Current water into the northern branch of the North Atlantic Current (NAC; Reverdin et al., 2003). It is modulated by changes in the SPG strength driven by changes in atmospheric forcing. Recently, Fox et al. (2022) highlighted that reduced surface heat loss led to an increase in warmer (less dense) waters in the Labrador Sea. The transport of these less dense waters from the upper ocean layers through the Labrador Current, along with reduced volume transport from the Gulf Stream, drove the cooling and freshening in the eastern subpolar region.

However, some studies suggest an important role for interactions between the subpolar North Atlantic and the Arctic. J. Zhang et al. (2021) and Sundby and Drinkwater (2007) attribute ESNA freshening events during 1983–1995 and 1947–2000 to the export of freshwater buildup in the Arctic. They suggest that sea ice and liquid freshwater anomalies travel via the Fram Strait and Davis Strait to the Labrador Sea and circulate around the eastern subpolar gyre in the North Atlantic Current. The proposed mechanism of freshwater buildup in the 1990s is increased freshwater flux from the Davis Strait (Belkin, 2004), which entered the Labrador Sea and propagated around the eastern subpolar gyre (Sundby & Drinkwater, 2007).

In this paper, we focus on what sets the upper ocean salinity in the ESNA on decadal time scales with emphasis on the two recent freshening events in the 1990s and 2010s using observations and modelling tools. We look at salt content anomaly budgets to explore oceanic mechanisms and further investigate the contribution of surface freshwater forcing in setting upper ocean salinity in the region.

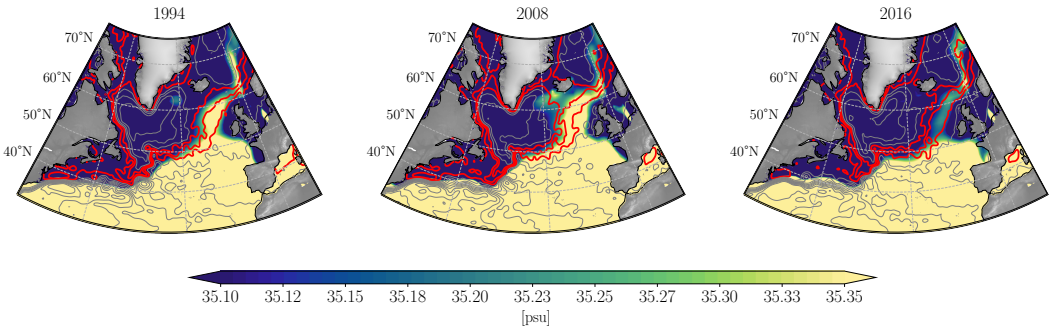

Figure 1: Annually-averaged subpolar North Atlantic upper-ocean salinity (0–200 m, colors) and sea-surface height (SSH; contours) averaged over one year preceding the salinity field. The SSH field is from the AVISO dataset and the salinity field is from the EN4 product. Following Chafik et al. (2019), the grey contours range from -0.8 m to 0.8 m with a spacing of 0.1 m and represent the mean dynamic topography (CNES-CLS2013 MDT). The red contours are -0.3, -0.2, -0.1 m and represent the three branches of the NAC. A Gaussian filter is used to smooth the SSH field with a scale of 1.25°. Modified from Fig. 3 of Weijer et al. (2022).

In section 2 we evaluate the ECCOv4r4 ocean state estimate using hydrographic sections and gridded salinity observations. In section 3, we compare and contrast the two fresh anomaly events observed during 1992–2017 using the gridded observations and the state estimate. We then diagnose the salinity variability using salt and salinity budget analysis with ECCOv4r4 for the entire subpolar North Atlantic (SPNA) and the ESNA in section 4. Potential mechanisms for the salinity variability through the lens of salinity and salt budgets are then discussed.

2 Evaluation of ECCOv4r4

The main tool for our analysis of upper ocean salinity is the ECCO (Estimating the Circulation and Climate of the Ocean) version 4 release 4 ocean state estimate (ECCOv4r4, Forget et al., 2015). The ECCOv4r4 state estimate is a dynamically-consistent, data-constrained solution of the MITgcm model for the period 1992–2017 (ECCO Consortium et al., n.d.). This allows for the construction of realistic closed budgets of volume, heat and salt. The horizontal resolution is 1°.

We utilize a number of observational datasets to evaluate ECCOv4r4, including the EN4 hydrographic dataset (Good et al., 2013), which is an observational product compiled by the UK Met office, and data from two hydrographic surveys. The OVIDE line (Daniault et al., 2016) is a combination of sections from the southern tip of Greenland to Portugal (Fig. 2b); we consider the occupation of this section from May to June 2016. The Extended ELLET line (Holliday & Cunningham, 2013) is a section from Iceland to Scotland (Fig. 2c); we consider the occupation of this section from June to July 2016. These are the same sections used by Holliday et al. (2020). Data from these hydrographic sections are compared with the monthly-mean ECCOv4r4 salinity anomaly.

Compared to the OVIDE section, model salinity in the Irminger Sea and the Iberian abyssal plain during summer of 2016 is realistic. The position of the 35.2 psu contour is similar in both ship-based and model derived sections (Fig. 2b). ECCOv4r4 also captures the sub-surface salinity minimum over the Iberian abyssal plain. However, ECCOv4r4 overestimates the 0–1000 m averaged salinity in the OVIDE section that lies insde the ESNA control volume (shown in Fig. 2a) by around 0.07 psu.

The upper 1000 m of the Rockall Trough has the highest salinity in the ELLET section in both observations and ECCOv4r4 (shown in Fig. 2c as salinity greater than 35.3 psu). However, ECCOv4r4 overestimates the salinity in the upper 1000 m; contours of 35.3 psu extend further westward in the model than the ship-based measurements. The salinity decreases below 1000m, which is seen in both the observations and ECCOv4r4 data. Overall, ECCOv4r4 overestimates the 0–1000 m averaged salinity along the ELLET section in the Iceland Basin by around 0.07 psu.

To quantify the temporal variability of salinity in the subpolar gyre we consider two regions: the ESNA is defined as a box over 10–30°W, 46–65°N (Fig. 2a) and the SPNA is defined as the North Atlantic between 45–65°N. The upper ocean is defined as the top 1000 m because salinity anomalies in the ESNA are vertically coherent up to a depth of 1000 m (see Supplemental Figure S1). Previous works investigating upper ocean salinity in the ESNA also consider the top 1000 m (Holliday et al., 2020), although some studies consider shallower layers (Koul et al., 2020; Fox et al., 2022). The time series of upper ocean salinity in the ESNA shows periods of freshening and salinification which are broadly consistent between ECCOv4r4 and EN4 (Fig. 3b).

The mean absolute salinity in the upper 1000 m ESNA is 35.34 $\pm$ 0.05 psu in EN4 and 35.28 $\pm$ 0.03 psu in ECCOv4r4, implying a very small mean salinity difference of 0.06 $\pm$ 0.06 psu. Additionally, the salinity biases between ECCOv4r4 and EN4 and hydrographic sections are significantly smaller than the salinity fluctuations. This builds confidence in the use of ECCOv4r4 for our analysis.

3 Salinity Anomalies in the Subpolar Gyre

In this section we consider the spatial and temporal structure of the fresh events in the subpolar region. We first establish the occurrence of two fresh anomalies in the upper 1000 m of the ESNA using the ECCOv4r4 and EN4 datasets. Time series of ESNA salinity anomalies (1992–2017) are computed from ECCOv4r4 and EN4 by averaging salinity over the top 1000 m and the ESNA region. We also remove the seasonal cycle and perform a linear detrending of the time series (Fig. 3b).

We observe a fresh anomaly in the ESNA in the early 1990s, after which there is a prolonged period of salinification until 2008, and a reversal to freshening thereafter. The salinity time series in EN4 exhibits more high frequency variations than ECCOv4r4, which may be explained both by interpolation of sparse data in EN4 and possibly muted variability in ECCOv4r4 due to its coarse resolution. A noticeable disagreement between EN4 and ECCOv4r4 occurs during 1995–1996, when the ESNA shows anomalous positive salinity anomalies in EN4, whereas ECCOv4r4 shows negative salinity anomalies (Fig. 3b). The reason for this difference is highlighted in the spatial maps of 0–1000 m salinity anomalies that show a large positive anomaly situated south of the Grand Banks in 1995 in both datasets (see Supplemental Figs. S2, S3). In EN4 this anomaly spreads throughout the ESNA in 1996, but it does not spread so far east in ECCOv4r4.

The first fresh anomaly event (F_1) is observed from 1992 until 1995 in EN4 and from 1992 to 1997 in ECCOv4r4. For the second fresh anomaly event (F_2), both datasets show the Iceland basin salinity anomaly dropping below zero after 2012 until 2017. This is also reflected in the upper ocean salinity anomaly maps in the ECCOv4r4 and EN4 datasets (see Supplemental Figs. S2–S3). We label the 1990s fresh event as F_1 and the 2010s fresh event as F_2.

Spatial trends in the upper ocean (0–1000 m) salinity are computed using EN4 and ECCOv4r4 (Fig. 3a). During 2005–16, both products show a statistically significant freshening in the ESNA at 95% confidence intervals using the student's t-distribution. ECCOv4r4 and EN4 disagree on trends in the Labrador Sea and the Grand Banks region, however (Fig. 3a).

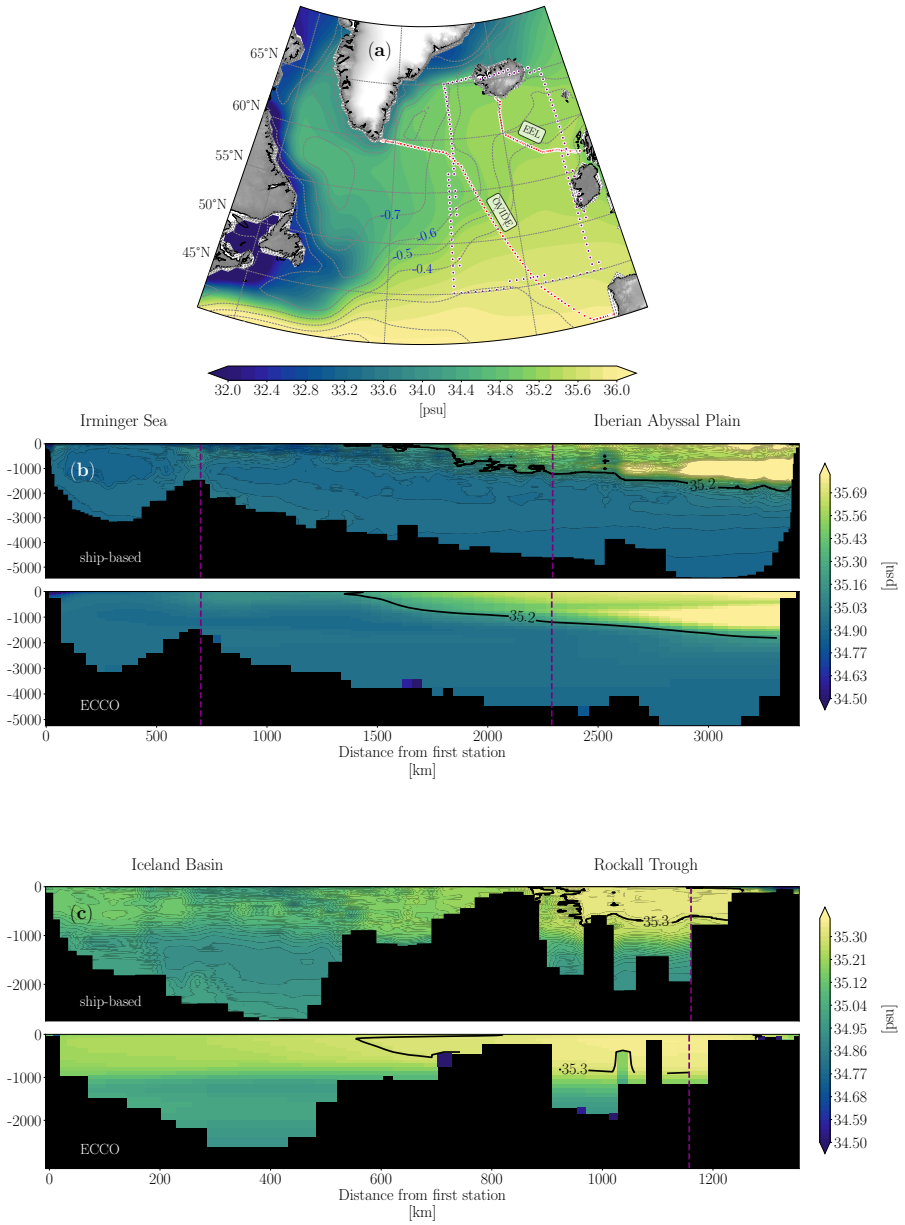

Figure 2: (a) Subpolar North Atlantic (SPNA) sea surface salinity field along with sea level height anomaly contours (spacing of 0.04 m) in the ECCOv4r4 dataset averaged over 1992–2017. The ESNA region (10–30°W, 46–65°N) is shown in purple and the Extended ELLET line (EEL) and OVIDE section are shown in red. (b-c) Comparison of ECCOv4r4 salinity for (b) June–July 2016 with the OVIDE section and (b) May–June 2016 with the ELLET line. The ECCOv4r4 salinity sections are taken at the same times as the field observations. Vertical purple lines indicate parts of the sections inside the ESNA control volume defined in (a) (for the OVIDE section 700–2290 km, and for the ELLET section 0–1150 km, are within the ESNA control volume). Colorbar limits and abscissa scales are different for the two section plots.

Next, we consider the annually averaged anomalies in the ECCOv4r4 data and compare the two fresh anomaly events, F_1 and F_2 (Fig. 4). As we trace the freshwater event

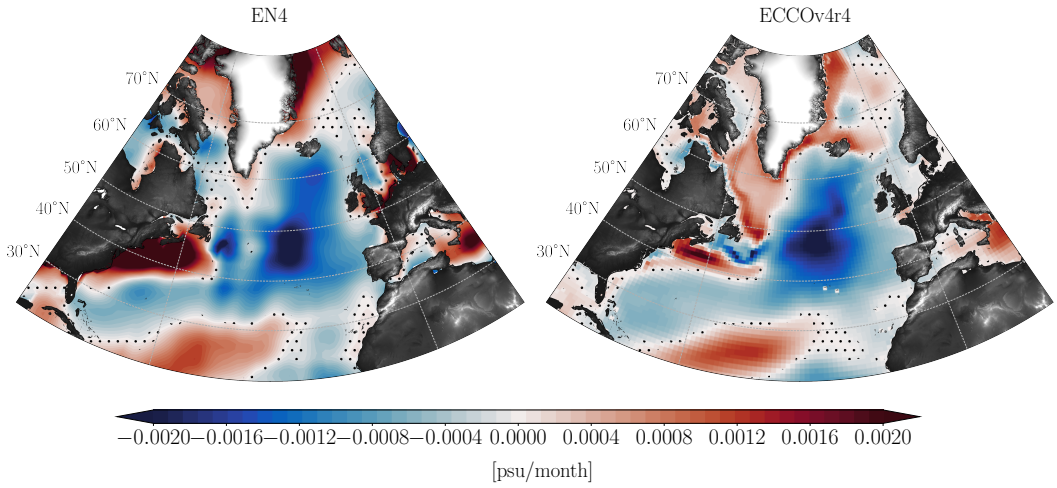

(**a**)

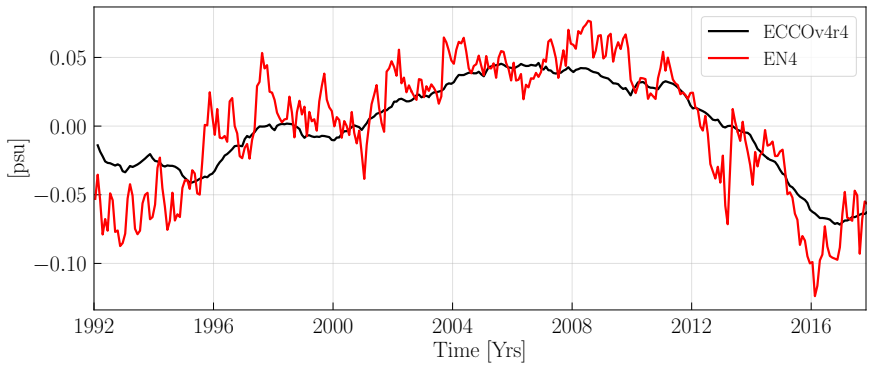

(**b**)

Figure 3: (a) Spatial distribution of linear trends in the upper-ocean salinity (0–1000 m) over 2005–2016 using monthly mean fields of EN4 and ECCOv4r4. Dotted regions display insignificant trends calculated using the students-t test with a p-value of 0.05. (b) Upper ocean 1000 m salinity anomaly time series for the eastern Subpolar North Atlantic (ESNA) from EN4 (red) and ECCOv4r4 (black) datasets. The ESNA is defined as 45–65°N, 10–30°W (purple box in Fig 2).

in the 1990s (F_1) we observe a fresh ESNA and saltier western subpolar gyre (SPG) in 1992. Fresh anomalies are situated in the Labrador Sea in 1993 and 1994 and in the Iceland Basin in 1995. By 1996, the signal fades away from the ESNA. The 2010s event has similar fresh anomalies in the Labrador Sea in 2013 and in the Iceland Basin in 2016. Note that in both events, there are positive salinity anomalies south of the Grand Banks region, preceding the maximum freshening in 1995 and 2016. Prior studies indicate anomalies of ocean properties of opposite signs between the Gulf Stream path and the subpolar gyre (Buckley et al., 2014; Joyce & Zhang, 2010; Sanchez-Franks & Zhang, 2015; Yeager, 2015; Hátún et al., 2009; R. Zhang, 2008; Nye et al., 2011; Yan et al., 2017, 2018).

We investigate this further using ECCOv4r4 by tracking salinity anomalies along the western SPG and along the Gulf Stream, with the Iceland Basin as a common terminus. We create a section following mean sea level anomaly contours around the sub-

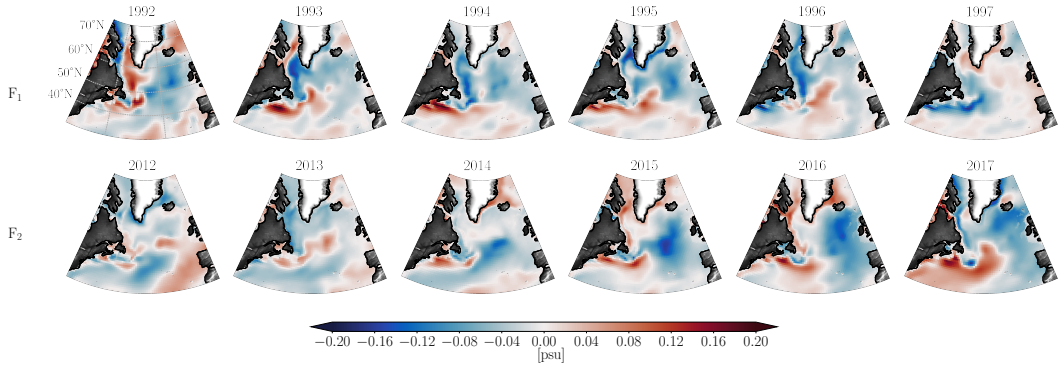

Figure 4: Annually averaged anomaly maps for the upper 1000 m salinity (0–1000 m) during 1992–1994 and 2012–2014 in ECCOv4r4.

polar gyre which begins south of Denmark Strait (Fig. 5a). The section follows the -0.8 m mean sea level anomaly contour along the East Greenland Current around the southeast coast of Greenland. The section continues along the West Greenland Current to the entrance of Baffin Bay (Davis Strait), where it retroflects and follows the Baffin Island Current, eventually reaching the Labrador Sea. At this point, the section follows the -0.5 m mean sea level anomaly contour as it retroflects east of the Flemish Cap and follows the path of the northern branch of the NAC to the Iceland basin. This section represents a potential subpolar pathway for the anomaly propagation.

To investigate the salinity anomalies along a potential subtropical pathway, we create a section along the Gulf Stream that also terminates in the Iceland Basin (Fig. 5a). Both sections are inspired by the Lagrangian studies carried out by Burkholder and Lozier (2014); Foukal and Lozier (2018); Koul et al. (2020); J. Zhang et al. (2021), in which passive tracers are tracked to the Iceland basin in a variety of experiments.

We first inspect the subtropical section. For both subpolar freshening events, there are positive salinity anomalies along the Gulf Stream path. The positive salinity anomaly signal south of the Grand Banks is also observed in the years preceding the fresh anomaly event in the annually averaged salinity anomaly maps (Fig. 4). Along the subpolar section, high frequency freshening/salinification events can be tracked from Denmark Strait along the East Greenland Current and West Greenland Current. Along the Labrador Current (from Davis Strait to the Grand Banks), the characteristics of the freshening/salinification events exhibit lower frequency variations than those seen along the East and West Greenland Currents. From the Grand Banks to the Iceland Basin, the freshening/salinification events occur at even lower frequencies. The relationship between salinity anomalies in the Icelandic Basin and those in the East/West Greenland Current and Labrador Current is complex, with some indications of signal propagation along the subpolar gye pathways, as suggested by Holliday et al. (2020) and Fox et al. (2022). There is no clear difference in the salinity anomalies along these sections for the two freshening events.

4 Salt Budget Analysis

We now explore the role of circulation changes quantitatively by constructing a salt mass budget for the region. We construct a budget of the salt mass, an extensive quantity, rather than salinity, an intensive quantity, because the salt budget can be closed with higher accuracy than the salinity budget. Additionally, considering salt budgets avoids the ambiguities associated with reference salinity for freshwater budgets (Schauer & Losch, 2019). As surface freshwater fluxes contain no salt, they do not play a role in the salt

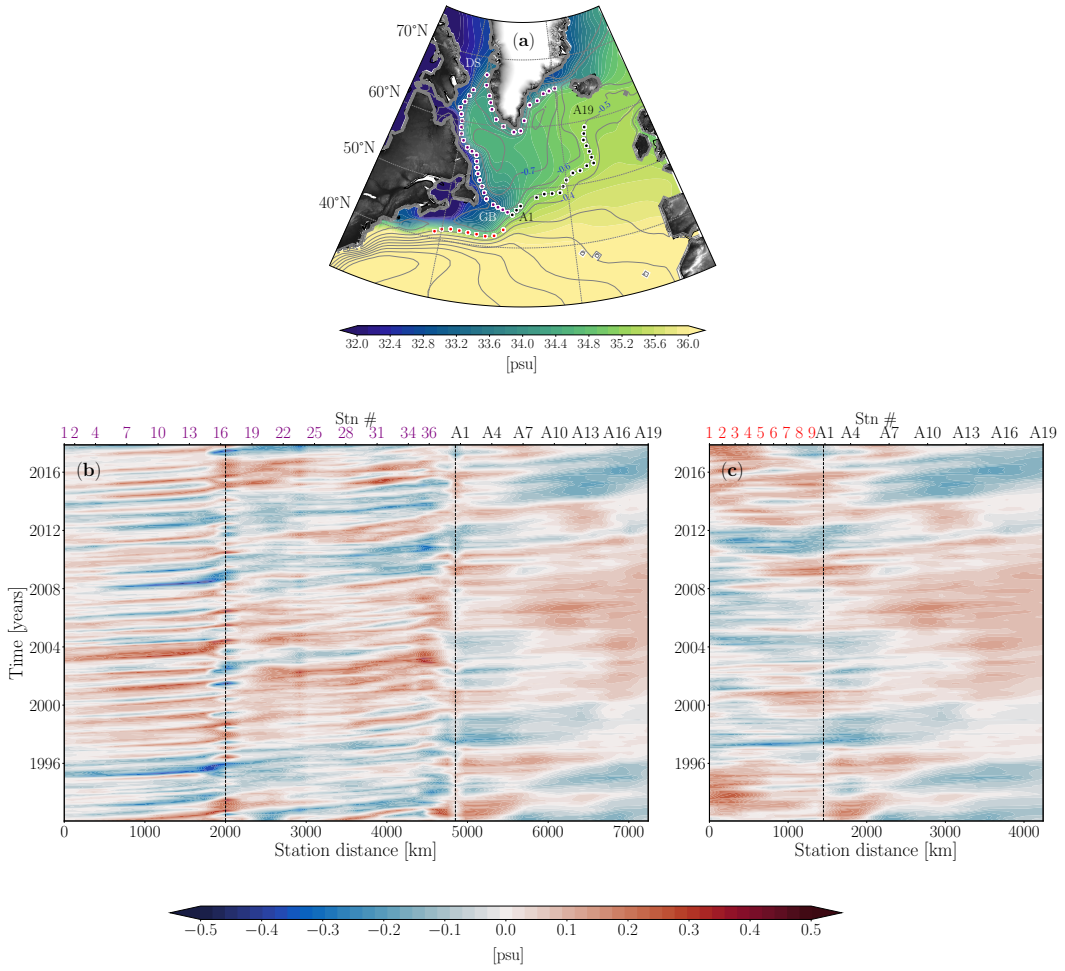

Figure 5: (a) Continuous sections along the western subpolar gyre boundary (purple; 56 stations) and along the Gulf Stream (red; 28 stations). The subtropical and subpolar sections intersect at the NAC (station A1) and both continue into the Iceland Basin (stations A1-A19, black dots). (b,c) Hovmöller diagrams of monthly salinity anomalies in the ECCOv4r4 data along the (b) subpolar and (c) subtropical sections. Vertical dashed lines are shown at Davis Strait (DS, black) and the Grand Banks (GB, black).

budget. The role of surface freshwater in the form of $P-E+R$ (Precipitation-Evaporation+Runoff) is analyzed separately in a salinity budget calculation in Section 5. The salt budget analysis builds on previous work investingating heat and salinity variability in the subpolar North Atlantic (Buckley et al., 2014, 2015; Piecuch et al., 2017; Oldenburg et al., 2018; Tesdal & Haine, 2020; Nguyen et al., 2021).

The salt conservation equation for the non-linear free surface in ECCOv4r4 is expressed in $z^\star$ coordinates (see equation (3) in Forget et al., 2015). In $z^\star$ coordinates, sea surface height variations, η, are proportionally divided between ocean layers: $z^\star = (z-\eta)/(H+\eta)$ (equation (1) in Piecuch, 2017), where z is the fixed vertical coordinate and H is the ocean depth.

We express the volume and time integrated salt content change from an initial time t_i, $M_s(t)$, for the control-volume V as

$$\underbrace{\rho_0 \int_{t^\star=t_i}^{t^\star=t_f} \int_V \frac{\partial(\eta^\star S)}{\partial t}\, dV^\star\, dt^\star}_{\text{Salt Mass}\equiv M_s(t)} = \underbrace{\rho_0 \int_{t^\star=t_i}^{t^\star=t_f} \int_V -\nabla_{z^\star}\cdot(\eta^\star S \mathbf{v}_{res}) - \frac{\partial(S w_{res})}{\partial z^\star}\, dV^\star\, dt^\star}_{\text{Advection}\equiv A(t)}$$
$$+ \underbrace{\rho_0 \int_{t^\star=t_i}^{t^\star=t_f} \int_V \eta^\star \mathcal{F}_S\, dV^\star\, dt^\star}_{\text{Forcing}\equiv F_s(t)} + \underbrace{\rho_0 \int_{t^\star=t_i}^{t^\star=t_f} \int_V \eta^\star (D_{\sigma,S} + D_{\perp,S})\, dV^\star\, dt^\star}_{\text{Diffusion}\equiv D(t)}. \quad (1)$$

In this equation $\eta^\star = 1 + \eta/H$ is a scaling factor, $\nabla_{z^\star}$ indicates the gradient at constant $z^\star$, $(\mathbf{v}_{res}, w_{res})$ are the residual velocity fields defined as the sum of the Eulerian and bolus (eddy-induced transport velocity) velocities, F_s is the forcing at the surface due to surface salt exchange due to sea ice melting/formation and a redistribution of the surface flux in the vertical column, and $D_{\sigma,S}$ and $D_{\perp,S}$ are diffusive processes parameterized along iso-neutral and vertical directions, respectively. See Appendix A for more details on the salt budget.

We consider V to be the upper 1000 m in the ESNA; we also consider the upper 1000 m for the whole SPNA. The integration depth is chosen to be 1000m because salinity anomalies are found to have strong vertical coherence over this depth (see Supplemental Fig. S1). Additionally, it is preferable to compute budgets for a layer that encompasses the wintertime mixed layer, as diffusive mixing will be a dominant term for layers that cut across the mixed layer (Buckley et al., 2014, 2015).

Eq. (1) expresses that the total time integrated salt mass change since t_i is balanced by the time integrated horizontal and vertical advective convergence of salt flux, diapycnal and isopycnal diffusion, and surface forcing. The four terms, $M_s(t)$, $A(t)$, $F_s(t)$, and $D(t)$, are each computed individually from the ECCOv4r4 output, which allows us to test the closure of (1). The ratio of the residual (left hand side minus right hand side) to the salt mass (left hand side) is of O(10^{-4}). Details on how to close the salt budget in the ECCOv4r4 dataset are provided in Piecuch (2017).

Time integration is done from $t_i = 1992$ to $t_f = 2017$. We remove the mean seasonal cycle and a linear trend from all terms in the time integrated salt budget (Eq. (1)) to yield anomalies of each of the budget terms, which we label as M_s', A', F_s', and D' (Fig. 6).

We observe a negative salt content anomaly (M_s') in both the SPNA and ESNA during 1992–1997 and 2012–2017 (Fig. 6). The salt mass anomaly increases starting in 1995 and reaches a maximum in 2007 for the entire SPNA and in 2008 for the ESNA. We find that the advection term (A') contributes almost entirely to the salt content anomaly, with the diffusion term (D') playing a minor role. The surface salt forcing (due to brine rejection, F_s') has a negligible impact. We highlight the years in yellow/blue when the advection term increases/decreases rapidly in the two basins.

In the following analysis, we further investigate the advection and diffusion terms. We decompose the anomalous advection (A') into terms related to the mean and time variable velocities and salinity, following Dong and Sutton (2002); Doney et al. (2007); Buckley et al. (2015); Piecuch et al. (2017) and Tesdal and Haine (2020). Overbars denotes time averaging, i.e $\bar{\mathbf{v}} = \frac{1}{(t_f - t_i)} \int_{t_i}^{t_f} \mathbf{v} dt$, and the prime denotes departure from the time average. The averaging period is 1992–2017. This decomposes the advection term into variability produced by changes in the circulation, variability produced by changes in salinity, and that due to the co-variability of the circulation with the salinity.

We now express $\mathbf{v}_{res} = \mathbf{v}_e + \mathbf{v}_b$, i.e., the total velocity is the sum of Eulerian ($\mathbf{v}_e$) and bolus ($\mathbf{v}_b$) velocities, and similarly for the vertical velocities ($w_{res} = w_e + w_b$). Re-

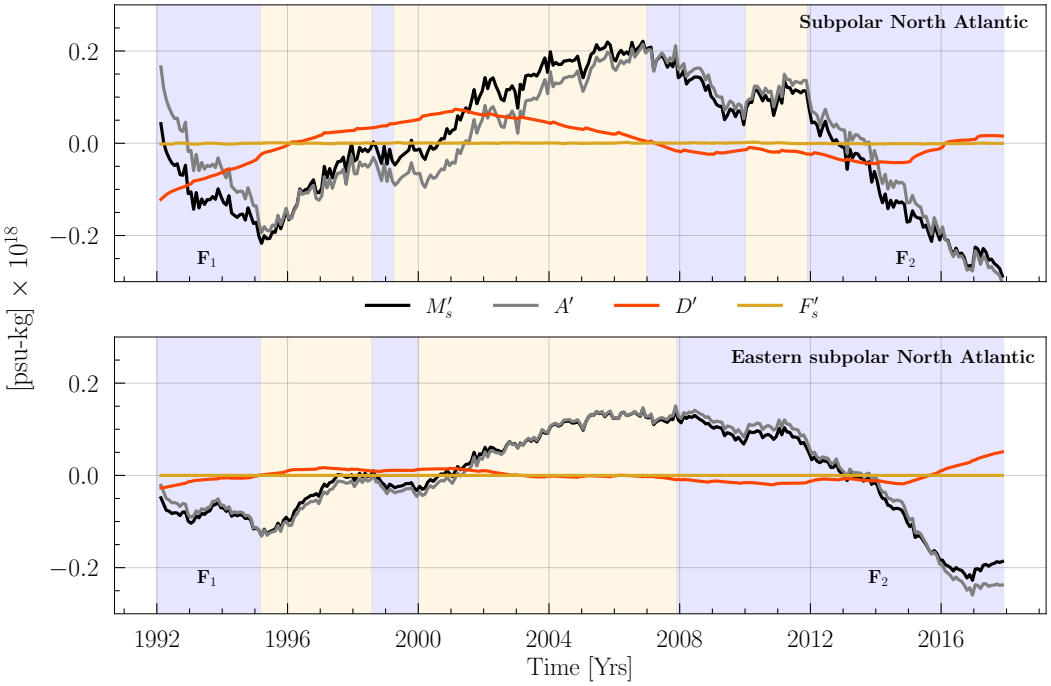

Figure 6: (a) Time and volume integrated salt anomaly budget for the upper 1000 m of the (a) SPNA and (b) the ESNA (see Fig. 2 for the definition of the ESNA). M'_s, A', F'_s, and D' are anomalies in salt mass content, salt advection, surface salt forcing, and total salt diffusion obtained after removing the mean seasonal cycle and a linear trend in the time integrated salt budget (Eq. (1)). F_1 and F_2 are fresh anomaly events in the two basins during 1992–1997 and 2012–2017, respectively. Yellow/blue shading indicates periods of increased/decreased advection of salt mass.

arranging the terms in Eq. (A2) gives:

$$
\begin{aligned}
A' = &\underbrace{-\rho_0 \int_{t^\star=t_i}^{t^\star=t_f} \int_V \left(\nabla_{z^\star} \cdot \eta^\star \bar{\mathbf{v}}_e S' + \frac{\partial(\bar{w}_e S')}{\partial z^\star} \right) dV^\star \, dt^\star}_{A_e^s} \\
&\underbrace{-\rho_0 \int_{t^\star=t_i}^{t^\star=t_f} \int_V \left(\nabla_{z^\star} \cdot \eta^\star \mathbf{v'}_e \bar{S} + \frac{\partial(w'_e \bar{S})}{\partial z^\star} \right) dV^\star \, dt^\star}_{A_e^v} \\
&\underbrace{-\rho_0 \int_{t^\star=t_i}^{t^\star=t_f} \int_V \left(\nabla_{z^\star} \cdot \eta^\star (\mathbf{v'}_e S' - \overline{\mathbf{v'}_e S'}) + \frac{\partial(w'_e S' - \overline{w'_e S'})}{\partial z^\star} \right) dV^\star \, dt^\star}_{A_e^{vs}} \\
&\underbrace{-\rho_0 \int_{t^\star=t_i}^{t^\star=t_f} \int_V \left(\nabla_{z^\star} \cdot \eta^\star \bar{\mathbf{v}}_b S' + \frac{\partial(\bar{w}_b S')}{\partial z^\star} \right) dV^\star \, dt^\star}_{A_b^s} \\
&\underbrace{-\rho_0 \int_{t^\star=t_i}^{t^\star=t_f} \int_V \left(\nabla_{z^\star} \cdot \eta^\star \mathbf{v'}_b \bar{S} + \frac{\partial(w'_b \bar{S})}{\partial z^\star} \right) dV^\star \, dt^\star}_{A_b^v} \\
&\underbrace{-\rho_0 \int_{t^\star=t_i}^{t^\star=t_f} \int_V \left(\nabla_{z^\star} \cdot \eta^\star (\mathbf{v'}_b S' - \overline{\mathbf{v'}_b S'}) + \frac{\partial(w'_b S' - \overline{w'_b S'})}{\partial z^\star} \right) dV^\star \, dt^\star}_{A_b^{vs}} + \epsilon. \qquad (2)
\end{aligned}
$$

The total advective salt transport convergence can be calculated exactly, as it is an output of ECCOv4r4. However, the separation of A' into terms related to the mean and time variable velocities and salinities requires an offline calculation using the monthly mean velocities and salinity (interpolated to the model velocity grid points). Thus, the calculation misses covariability between salinity and velocity on sub-monthly timescales (Tesdal & Abernathey, 2021), which leads to a residual term which we call ϵ. The residual term ϵ is small compared to other terms in the salt budget (see Fig. 7); ratios of ϵ to each individual term are $O(10^{-1})$.

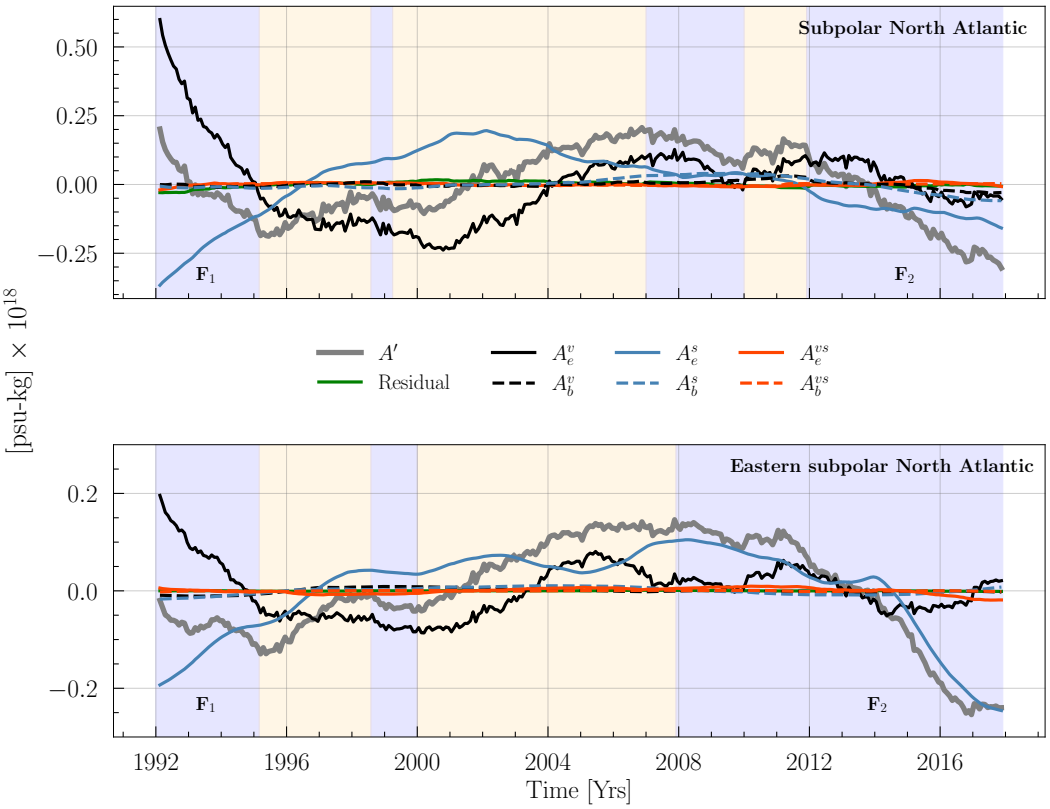

Figure 7: Decomposition of the anomalous advection term A' in the salt budget for the upper 1000 m of the (a) SPNA and (b) ESNA. The A' term is decomposed into contributions from: changes in the Eulerian (A_e^v) and bolus (A_b^v) circulation, changes in the salinity along mean Eulerian (A_e^s) and bolus (A_b^s) circulation, and changes due to the co-variability of the Eulerian (A_e^{vs}) and bolus (A_b^{vs}) circulation with the salinity. See Eq. (2) for details on the terms. F_1 and F_2 are fresh anomaly events in the two basins during 1992–1997 and 2012–2017, respectively. Yellow/blue shading indicates periods of increased/decreased advection of salt mass.

For the whole SPNA, during the F_1 event, the variability in the advective convergence term is dominated by the anomalous Eulerian advection of mean salinity (A_e^v, Fig. 7). During 1992–1995, it is twice that of the mean circulation of anomalous salinity (A_e^s). For the F_2 event, the mean Eulerian circulation of anomalous salinity (A_e^s) and the anomalous Eulerian circulation of mean salinity (A_e^v), both have approximately equal contributions in driving the freshening (Fig. 7). Note that A_e^v and A_e^s are anti-correlated in most parts during 1992–2017. Anti-correlation of advective convergences due to salinity variations and due to geostrophic velocity variations is expected when isobars and isohalines are aligned. Analogous results related to heat transport convergences are shown

by Buckley et al. (2015). The bolus terms A_b^v and A_b^s are also mostly anti-correlated during 1992–2017, which is expected according to the Gent-McWilliams parameterization if isoneutral slopes are aligned with isohalines.

The decomposition of the anomalous advection term for the ESNA differs from that of the full SPNA. The F_1 negative salt anomaly is still dominated by the anomalous circulation of mean salinity (A_e^v). In contrast, the driver for the F_2 anomaly is the mean circulation of anomalous salinity (A_e^s). Also, unlike the SPNA, A_e^v and A_e^s are not anticorrelated. This indicates that either (1) the isobars and isohalines are not strongly aligned, which would occur if the density field in the ESNA is only weakly dependent on salinity, or (2) there is a strong contribution of agoestrophic transports to the advective convergences. For example, there is no expected anticorrelation between salt transport convergences due to salinity variations and those due to Ekman transport variations. Buckley et al. (2015) show that the ESNA is a region where the variance of Ekman heat transport convergence exceeds geostrophic heat transport convergence (their Figure 1c,d), and anticorrelations between advective ocean heat transport convergences due to temperature and velocity variations are modest (their Figure 4c).

Note that in event F_2, A_e^s plays a substantial role in the reduced salt content in the ESNA. Thus, we explore the origin of this term more fully by determining which boundary of the SPNA box dominates the A_e^s term. We apply the Gauss-divergence theorem to rewrite the term A_e^s (Eq. (1)) as surface integrals rather than volume integrals. The A_e^s term can be then expressed as:

$$A_e^s = \underbrace{-\rho_0 \int_{t^\star=t_i}^{t^\star=t_f} \int_B [(\eta^\star \bar{\mathbf{v}}_e S') \cdot \hat{\mathbf{n}}]\, dB^\star\, dt^\star}_{v_e^s|_{south}+v_e^s|_{north}+v_e^s|_{east}+v_e^s|_{west}} \underbrace{- \rho_0 \int_{t^\star=t_i}^{t^\star=t_f} \int_{bottom} \bar{w}_e S'\, dB^\star\, dt^\star}_{v_e^s|_{bottom}}. \quad (3)$$

Here, B represents the four vertical boundaries of the box, i.e., south, north, east and west; and bottom represents the horizontal boundary at 1000 m. The contributions to

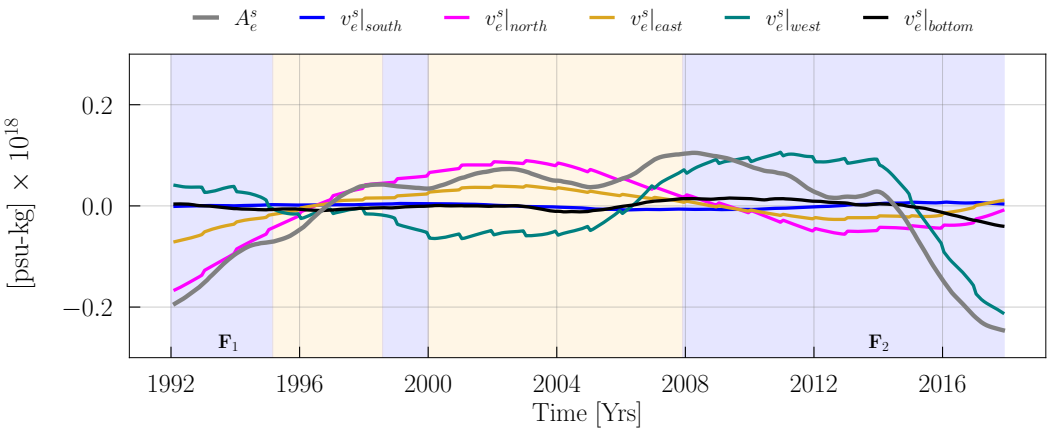

Figure 8: Contribution to changes in anomalous salt flux in the ESNA due to changes in salinity along mean flow (A_e^s) as a sum of salt fluxes across lateral boundaries and across the 1000 m bottom boundary. See Eqs. (2) and (3) for details on the terms, and see also Fig. 6 for information on the full salt budget. F_1 and F_2 are fresh anomaly events in the two basins during 1992–1997 and 2012–2017, respectively. Yellow/blue shading indicates periods of increased/decreased advection of salt mass.

A_e^s from each of the boundaries are shown in Fig. 8. Recall, that during F_2, A_e^s is the

dominant term leading to the decrease in salt content. During F_2, the anomalous Eulerian salt flux entering the western boundary ($v_e^s|_{west}$) is the primary contribution to A_e^s. It is responsible for bringing fresher water along the mean NAC. This is in contrast to the F_1 event where the advection is driven by the A_e^v term and the A_e^s opposes the salt content decrease.

The anomalous diffusion component of the salt mass anomaly budget is expressed as

$$D' = \underbrace{\rho_0 \int_{t^\star=t_i}^{t^\star=t_f} \int_V \eta^\star D_{\sigma,S}\, dV^\star dt^\star}_{D_H} + \underbrace{\rho_0 \int_{t^\star=t_i}^{t^\star=t_f} \int_V \eta^\star D_{\perp,S}\, dV^\star dt^\star}_{D_V}. \tag{4}$$

In both the ESNA and the SPNA, the horizontal diffusion dominates vertical diffusion across 1000 m (Fig. 9). Vertical diffusion is expected to be small outside the mixed layer, which is less than 1000 m for the area averaged ESNA and SPNA.

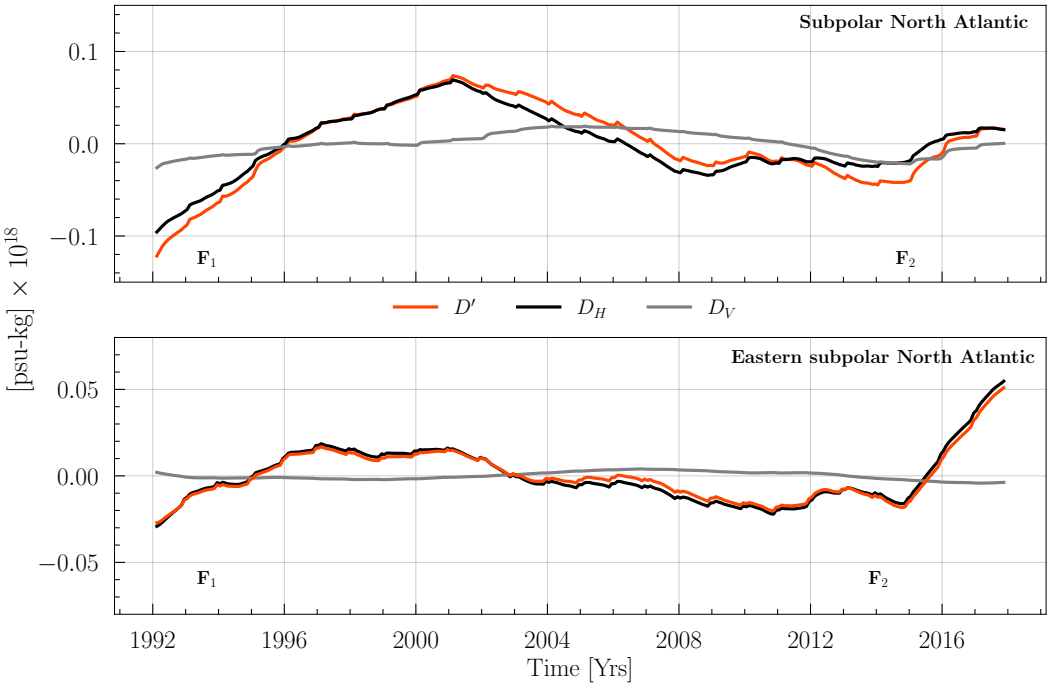

Figure 9: Decomposition of the diffusion term (D') in the anomalous salt mass budget for the upper 1000 m of the (a) SPNA and (b) ESNA. Decomposition terms include horizontal (D_H) and vertical diffusion (D_V), as in Eq. (4). F_1 and F_2 are fresh anomaly events in the two basins during 1992–1997 and 2012–2017, respectively.

In summary, for salt budgets over the top 1000 m of the ESNA and SPNA, the advective ocean salt transport convergence dominates the salt content anomalies and diffusion plays a lesser role. Due to the shallower mixed layers in the ESNA as compared to the full SPNA, diffusion plays a lesser role in the ESNA than the SPNA. During event F1, the advective salt transport convergence is mostly determined by circulation anomalies acting on the mean salinity field in both the ESNA and the SPNA. During F2, the reduced salt content is determined by the mean circulation acting on salinity gradient anomalies. For the SPNA, both the Eulerian mean (A_e^s) and bolus (A_b^s) term are important whereas in the ESNA only the Eulerian mean term (A_e^s) plays a role. In the ESNA

the term A_e^s is primarily related to transports across the western boundary, related to salinity anomalies being advected along the mean NAC.

5 Role of Precipitation, Evaporation, and Runoff

Performing a salt budget analysis for a control volume in the ocean does not account for changes in the salinity due to surface freshwater exchange, i.e., precipitation (P), evaporation (E), and runoff (R). To account for freshwater forcing from the atmosphere, ECCOv4r4 provides a diagnostic representing $P-E$ fluxes and freshwater input from river runoff, R. We use the seawater volume budget and the salt budget to estimate the contribution of $P-E+R$ in changing the salinity in the ESNA and SPNA.

The volume conservation in ECCOv4r4 is (see equation (3) in Forget et al., 2015)

$$\frac{1}{H}\frac{\partial \eta}{\partial t} = -\nabla_{z^\star} \cdot \eta^\star \mathbf{v}_e - \frac{\partial w}{\partial z^\star} + \eta^\star \mathcal{F}. \tag{5}$$

Here, η is the sea surface height, $\mathbf{v_e} = (u_e, v_e, w_e)$ are the horizontal and vertical Eulerian velocity components, and $\mathcal{F}$ is the surface freshwater forcing term due to $P-E+R$. The other terms are the same as those in Eq. (A1). Eq. (5) expresses that the rate of change of the volume is a sum of surface freshwater forcing and advective volume-flux divergence. Integration of Eq. (5) in space and time is used to calculate the volume-integrated anomaly in the total mass of the ESNA and SPNA (ECCOv4r4 makes the Boussinesq approximation, so seawater volume is proportional to seawater mass). As in Eq. (1), we express this as

$$\underbrace{\int_{t^\star=t_i}^{t^\star=t_f} \int_V \rho_0 \, dV^\star \, dt^\star}_{\text{Seawater Mass} \equiv M(t)} = \underbrace{\rho_0 \int_{t^\star=t_i}^{t^\star=t_f} \int_V -\nabla_{z^\star} \cdot (\eta^\star \mathbf{v}_e) - \frac{\partial (w)}{\partial z^\star} \, dV^\star \, dt^\star}_{\text{Advection} \equiv A_w(t)}$$
$$+ \underbrace{\rho_0 \int_{t^\star=t_i}^{t^\star=t_f} \int_V \eta^\star \mathcal{F} \, dV^\star \, dt^\star}_{\text{Forcing} \equiv F(t)}. \tag{6}$$

Similar to the salt mass anomaly analysis, we remove the seasonality and long term trends from each term in Eq. (6) to give M', A'_w, and F', which are shown in Fig. 10. We find that the total mass (M') of the SPNA and the ESNA does not change significantly over 1992–2017. This is due to a compensation between the anomalous freshwater forcing (F') and the convergence of mass (A'_w) over the basins. Josey and Marsh (2005) and Holliday et al. (2020) show that the ESNA received anomalous positive $P-E+R$ during 1992–1999 and 2012–2017 (mainly as precipitation P). This is balanced by an increased mass flux exiting the basin during the same period.

We now decompose the total contribution to changes in the average salinity of the control volume using a combination of the salt mass and seawater mass budget. We express the salt tendency in the salt conservation equation using

$$\frac{\partial (\eta^\star S)}{\partial t} = \eta^\star \frac{\partial S}{\partial t} + S \frac{\partial \eta^\star}{\partial t} \tag{7}$$

and

$$\frac{\partial \eta^\star}{\partial t} = \frac{1}{H}\frac{\partial \eta}{\partial t} \tag{8}$$

(from the definition of $\eta^\star$). Along with Eq. (5), we can rewrite the salt conservation equation (A1) as an equation for the tendency of salinity (similar to equation (12) in Piecuch, 2017). We then express the time integrated salinity, $S(t)$, averaged over the control vol-

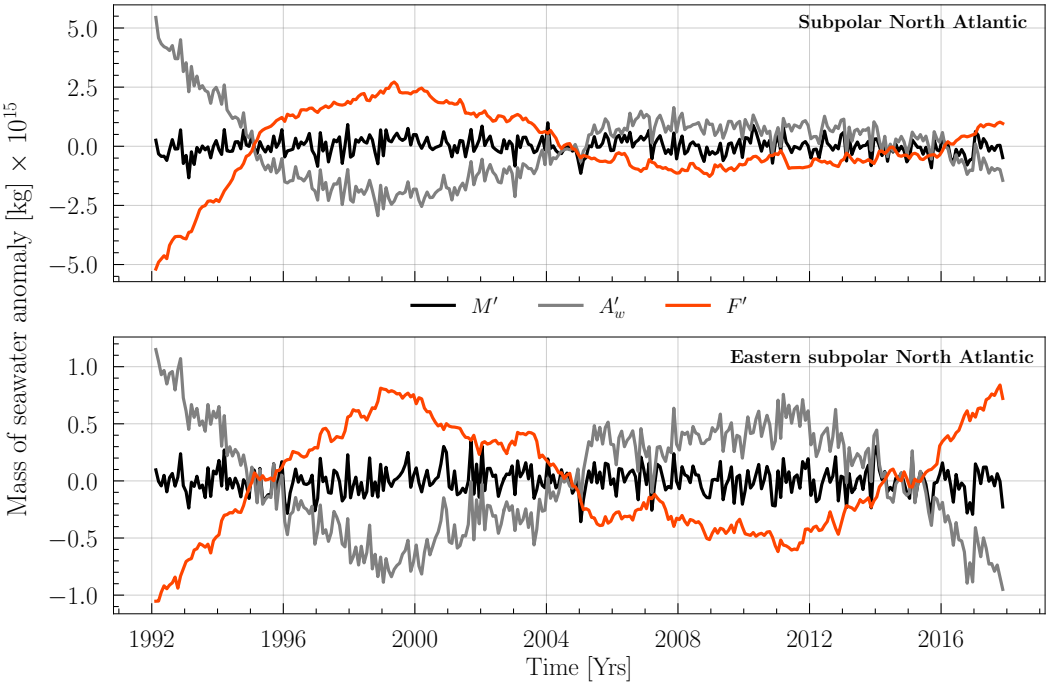

Figure 10: (a) Seawater mass anomaly budget for the upper 1000 m of the (a) SPNA and (b) ESNA. M', A'_w, and F' are anomalies in seawater mass, advection, and surface freshwater forcing, respectively, obtained after removing the mean seasonal cycle and a linear trend in the time integrated salt budget (Eq. (6)). F_1 and F_2 are fresh anomaly events in the two basins during 1992–1997 and 2012–2017, respectively.

ume V as

$$\underbrace{\frac{1}{V}\int_{t^\star=t_i}^{t^\star=t_f}\int_V \frac{\partial S}{\partial t}\,dV^\star\,dt^\star}_{S(t)} = \underbrace{\frac{1}{V}\int_{t^\star=t_i}^{t^\star=t_f}\int_V (D_{\sigma,S}+D_{\perp,S})\,dV^\star\,dt^\star}_{S_{Diff.}}$$
$$+\underbrace{\frac{1}{V}\int_{t^\star=t_i}^{t^\star=t_f}\int_V \frac{1}{\eta^\star}\left[S\nabla_{z^\star}\cdot(\eta^\star\mathbf{v}_e)+S\frac{\partial w}{\partial z^\star}-\nabla_{z^\star}\cdot(\eta^\star S\mathbf{v}_{res})-S\frac{\partial w_{res}}{\partial z^\star}\right]dV^\star\,dt^\star}_{S_{Adv.}}$$
$$+\underbrace{\frac{1}{V}\int_{t^\star=t_i}^{t^\star=t_f}\int_V (F_s-SF)\,dV^\star\,dt^\star}_{S_{Atm.}}. \quad (9)$$

We remove the seasonality and long term trends from each term in Eq. (9) to get the terms S', $S'_{Diff.}$, $S'_{Adv.}$, and $S_{Atm.}$, which are shown in Fig. 11. We find that salinity changes in both the SPNA and ESNA are controlled by ocean advection. The diffusion and surface forcing terms balance each other out. This suggests that salinity changes occurring due to $P-E+R$ are transported into the ocean interior via diffusion. We observe that precipitation plays a larger role during F_1 relative to F_2. Josey and Marsh (2005) and Holliday et al. (2020) conclude the same for the Iceland basin.

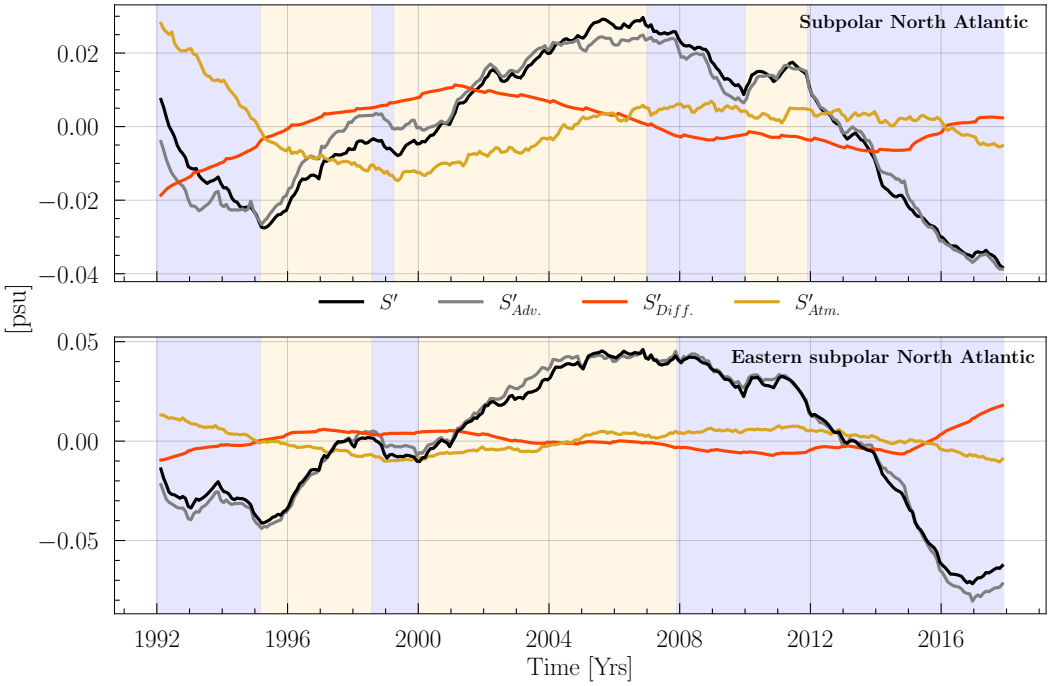

Figure 11: Salinity anomaly (S') contribution from the atmosphere ($S'_{Atm.}$), ocean advection ($S'_{Adv.}$) and diffusion ($S'_{Diff.}$) for the upper 1000 m of the (a) SPNA and (b) ESNA. See Eq. (9) for details of the salinity anomaly budget terms. F_1 and F_2 are fresh anomaly events in the two basins during 1992–1997 and 2012–2017, respectively. Yellow/blue shading indicates periods of increased/decreased advection of salt mass.

6 Discussion

In this study we investigate the cause of two low salinity events in the eastern subpolar North Atlantic (ESNA) and entire subpolar North Atlantic (SPNA): one during the 1990s (F_1) and one in the 2010s (F_2). The Great Salinity Anomaly (GSA) event (F_1) as described in Belkin (2004) propagates via the Labrador Sea and into the Iceland Basin in the mid 1990s. The fresh anomaly observed in the ESNA in the mid 2010s (F_2) has similar spatial characteristics.

Using salt mass budget analysis in the ECCOv4r4 state estimate, we show that for both events, and over the full period analyzed (1992–2017), salt content changes are dominated by changes in advective salt transport convergences, with a smaller role for diffusive transport convergences and a negligible role for salt fluxes related to sea ice formation/melting. However, the nature of the advective salt transport convergences differs between the two events:

1. The fresh anomaly in the 1990s (F_1) occurs due to anomalous circulation of mean salinity (A_e^v).
2. The fresh anomaly during 2012–2017 (F_2) is due to the mean circulation of anomalous salinity (A_e^s). This is entirely due to transport across the western face ($A_e^s|_{west}$) of the Iceland Basin (Fig. 8).
3. Vertical diffusive flux across the 1000 m depth boundary does not play a significant role in contributing to salinity changes.

These results are consistent with those of Fox et al. (2022) who argue that the recent freshening in the ESNA is due to anomalous advection of lighter waters originating in the Labrador sea. Note, however, that their Lagrangian particle tracking methodology is different from the Eulerian budget methodology used here (among other differences), which complicates a direct comparison of results.

Differences between the freshening in the ESNA and the entire SPNA are observed in the mean Eulerian circulation of anomalous salinity (A_e^s; Fig. 7). Integrated over the SPNA, A_e^s shows a steady decline from 2002–2017, whereas in the ESNA the steady decline begins in 2008 and then a sharp decline is observed during 2014–2016, thus driving the F_2 event.

The role of surface freshwater fluxes ($P-E+R$) is examined using a salinity budget. Freshwater forcing plays a modest role in the salinity budget, and the freshwater forcing is generally balanced by diffusive convergences. The anticorrelation between freshwater forcing and diffusive transports is due to the vertical redistribution of freshwater forcing, which occurs mainly over the mixed layer. The contribution of freshwater forcing and diffusive transports is larger in the SPNA than the ESNA due to the deeper mixed layers in the western basin. The surface freshwater fluxes ($P - E + R$) play a minor role in enhancing the fresh anomalies in the ESNA during the F_2 event. This was also noted by Holliday et al. (2020).

Holliday et al. (2020) state that the 2010s (F_2) event does not share the same characteristics of the 20th century GSAs. They argue that the precursor to this event shows no freshening in the Labrador Sea, unlike previous GSAs (Belkin, 2004; Sundby & Drinkwater, 2007). However, in the ECCOv4r3 freshwater budget for the Labrador Sea explored by Tesdal and Haine (2020) there is an increased freshwater flux from the Labrador Sea via the Labrador Current. This compensates an increased freshwater flux across the Davis Strait so that little net salinity change occurs in the Labrador Sea over this period. Recent papers argue that the 2010s (F_2) freshening event resembles a GSA in terms of a record salinity decrease in the ESNA. Specifically, Devana et al. (2021) observe that salinity decrease from November 2015 to March 2017 in the Iceland-Scotland Overflow Water is similar to the freshening observed in the 1990s. Also, Biló et al. (2022) note that the salinity decrease during 2016–2019 in the Irminger Sea (0.04 psu year^{-1}), following the freshening in the Iceland basin, is among the highest ever recorded.

Realistic, physically-consistent state estimates, such as ECCOv4r4 used here, are valuable to diagnose mechanisms of large-scale inter-annual salinity and temperature fluctuations because closed volume, heat, and salt budgets can be constructed. Apart from possible bias (section 2), such state estimates have some drawbacks, however. State estimates do not include error estimates in the model output fields, for instance (Piecuch et al., 2017). Tesdal and Haine (2020) address this issue by using ± 2 standard deviations of the monthly lateral ECCOv4r4 fluxes as a substitute for formal uncertainty estimates. Another limitation is that state estimates typically span a relatively short period (1992–2017 in the case of ECCOv4r4). Therefore, investigations of low-frequency (decadal to centennial) salinity and temperature variability are not yet possible with these products. Coupled climate models are a promising resource for these studies because they also allow construction of closed volume, heat, and salt budgets, but with much longer duration.

7 Data Availability Statement

We use an open source python package, OceanSpy (`https://oceanspy.readthedocs.io`; Almansi et al., 2019), to create and analyze synthetic hydrographic sections in the model data. We also use the python package gcm-filters (`https://gcm-filters.readthedocs.io`; Loose et al., 2022) to apply spatial Gaussian filters for smoothing the AVISO data.

The ECCOv4r4 dataset is publicly available on the SciServer system (Medvedev et al., 2016) and at `https://podaac.jpl.nasa.gov/ECCO`. The EN4 data are available at `www.metoffice.gov.uk/hadobs/en4/`. Python scripts with Juptyer notebooks used for analyzing ECCOv4r4 budgets can be accessed at `https://github.com/asiddi24/Siddiqui_et_al_JGR_Oceans_2024` along with scripts used for generating all figures in the manuscript.

Appendix A Salt Budget Equations

This appendix clarifies the formulation of Eqs. (1)–(3). The $z^\star$ coordinate is used in ECCOv4r4 to allow for exact tracer conservation (Campin et al., 2004) and to improve representation of flow over steep topography (Adcroft & Campin, 2004). Physically, $z^\star$ allows for variations in the non-linear free surface to be distributed throughout the vertical water column. Using this coordinate, Forget et al. (2015) express the salt conservation equation as

$$\frac{\partial(\eta^\star S)}{\partial t} = -\nabla_{z^\star} \cdot (\eta^\star S \mathbf{v}_{res}) - \frac{\partial(S\, w_{res})}{\partial z^\star} + \eta^\star (F_S + D_{\sigma,S} + D_{\perp,S}). \tag{A1}$$

Integrating Eq. (A1) over a spatial domain V and over time yields a time series for the salt mass, $M_s(t)$, expressed in Eq. (1).

For the anomalous advection term, A', consider

$$\begin{aligned} \mathbf{v}_{res} &= \bar{\mathbf{v}}_{res} + \mathbf{v'}_{res}, \\ w_{res} &= \bar{w}_{res} + w'_{res}, \\ S &= \bar{S} + S', \end{aligned}$$

This decomposition implies that

$$\begin{aligned} \bar{\mathbf{v}}_{res}\bar{S} &= \overline{\mathbf{v}_{res}S} - \overline{\mathbf{v'}_{res}S'}, \\ \bar{w}_{res}\bar{S} &= \overline{w_{res}S} - \overline{w'_{res}S'}. \end{aligned}$$

The anomalous advection term is therefore:

$$\begin{aligned} A' = -\rho_0 \int^t \int_V \nabla_{z^\star} \cdot \left[\left(\eta^\star (\bar{\mathbf{v}}_{res} S' + \mathbf{v'}_{res} \bar{S} + \mathbf{v'}_{res} S' - \overline{\mathbf{v'}_{res} S'} \right) \right] \, dV^\star \, dt^\star \\ - \rho_0 \int^t \int_V \frac{\partial (\bar{w}_{res} S' + w'_{res} \bar{S} + w'_{res} S' - \overline{w'_{res} S'})}{\partial z^\star} \, dV^\star \, dt^\star. \end{aligned} \tag{A2}$$

Applying the Gauss-divergence theorem, this can be re-written as

$$\begin{aligned} A' = -\rho_0 \int^t \int_B [\eta^\star \bar{\mathbf{v}}_{res} S' + \bar{w}_{res} S' + \eta^\star \mathbf{v'}_{res} \bar{S} + w'_{res} \bar{S} + \\ \eta^\star (\mathbf{v'}_{res} S' - \overline{\mathbf{v'}_{res} S'}) + (w'_{res} S' - \overline{w'_{res} S'}) \cdot \hat{\mathbf{n}}] \, dB \, dt^\star. \end{aligned} \tag{A3}$$

This is rearranged in Eq. (2).

Acknowledgments

The authors thank Renske Gelderloos, Miguel Jimenez-Urias, Wenrui Jiang and Anand Gnanadesikan for providing invaluable feedback through group discussions at various stages of the manuscript. We also thank Jan-Erik Tesdal for his input on ECCOv4r4 budget closures. Alan Fox and two anonymous reviewers provided constructive comments. This work was partially supported by award 80NSSC20K0823 from the National Aeronautics and Space Administration and by award 2242033 from the National Science Foundation.

References

Adcroft, A., & Campin, J.-M. (2004). Rescaled height coordinates for accurate representation of free-surface flows in ocean circulation models. *Ocean Modelling*, *7*(3), 269-284. doi: https://doi.org/10.1016/j.ocemod.2003.09.003

Almansi, M., Gelderloos, R., Haine, T. W. N., Saberi, A., & Siddiqui, A. H. (2019). Oceanspy: A Python package to facilitate ocean model data analysis and visualization. *Journal of Open Source Software*, *4*(39), 1506. doi: https://doi.org/10.21105/joss.01506

Belkin, I. M. (2004). Propagation of the Great Salinity Anomaly of the 1990s around the northern North Atlantic. *Geophysical Research Letters*, *31*(8). doi: https://doi.org/10.1029/2003GL019334

Belkin, I. M., Levitus, S., Antonov, J., & Malmberg, S.-A. (1998). Great Salinity Anomalies in the North Atlantic. *Progress in Oceanography*, *41*(1), 1 - 68. doi: https://doi.org/10.1016/S0079-6611(98)00015-9

Biló, T. C., Straneo, F., Holte, J., & Le Bras, I. A.-A. (2022). Arrival of New Great Salinity Anomaly Weakens Convection in the Irminger Sea. *Geophysical Research Letters*, *49*(11), e2022GL098857. (e2022GL098857 2022GL098857) doi: https://doi.org/10.1029/2022GL098857

Bryden, H. L., Johns, W. E., King, B. A., McCarthy, G., McDonagh, E. L., Moat, B. I., & Smeed, D. A. (2020). Reduction in Ocean Heat Transport at 26°N since 2008 Cools the Eastern Subpolar Gyre of the North Atlantic Ocean. *Journal of Climate*, *33*(5), 1677 - 1689. doi: https://doi.org/10.1175/JCLI-D-19-0323.1

Buckley, M. W., Ponte, R. M., Forget, G., & Heimbach, P. (2014). Low-Frequency SST and Upper-Ocean Heat Content Variability in the North Atlantic. *Journal of Climate*, *27*(13), 4996 - 5018. doi: https://doi.org/10.1175/JCLI-D-13-00316.1

Buckley, M. W., Ponte, R. M., Forget, G., & Heimbach, P. (2015). Determining the Origins of Advective Heat Transport Convergence Variability in the North Atlantic. *Journal of Climate*, *28*(10), 3943 - 3956. doi: https://doi.org/10.1175/JCLI-D-14-00579.1

Burkholder, K. C., & Lozier, M. S. (2014). Tracing the pathways of the upper limb of the North Atlantic Meridional Overturning Circulation. *Geophysical Research Letters*, *41*(12), 4254-4260. doi: https://doi.org/10.1002/2014GL060226

Campin, J.-M., Adcroft, A., Hill, C., & Marshall, J. (2004). Conservation of properties in a free-surface model. *Ocean Modelling*, *6*(3), 221-244. doi: https://doi.org/10.1016/S1463-5003(03)00009-X

Chafik, L., Nilsen, J. E. Ø., Dangendorf, S., Reverdin, G., & Frederikse, T. (2019). North atlantic ocean circulation and decadal sea level change during the altimetry era. *Scientific reports*, *9*(1), 1–9. doi: https://doi.org/10.1038/s41598-018-37603-6

Daniault, N., Mercier, H., Lherminier, P., Sarafanov, A., Falina, A., Zunino, P., ... Gladyshev, S. (2016). The northern North Atlantic Ocean mean circulation in the early 21st century. *Progress in Oceanography*, *146*, 142-158. doi: https://doi.org/10.1016/j.pocean.2016.06.007

Devana, M. S., Johns, W. E., Houk, A., & Zou, S. (2021). Rapid freshening of iceland scotland overflow water driven by entrainment of a major upper ocean salinity anomaly. *Geophysical Research Letters*, *48*(22), e2021GL094396. (e2021GL094396 2021GL094396) doi: https://doi.org/10.1029/2021GL094396

Dickson, R. R., Meincke, J., Malmberg, S.-A., & Lee, A. J. (1988). The great salinity anomaly in the Northern North Atlantic 1968-1982. *Progress in Oceanography*, *20*(2), 103 - 151. doi: https://doi.org/10.1016/0079-6611(88)90049-3

Doney, S. C., Yeager, S., Danabasoglu, G., Large, W. G., & McWilliams, J. C. (2007). Mechanisms Governing Interannual Variability of Upper-Ocean Tem-

perature in a Global Ocean Hindcast Simulation. *Journal of Physical Oceanography*, *37*(7), 1918 - 1938. doi: https://doi.org/10.1175/JPO3089.1

Dong, B., & Sutton, R. (2002). Variability in North Atlantic heat content and heat transport in a coupled ocean–atmosphere GCM. *Climate Dynamics*, *19*(5–6), 485–497. doi: https://doi.org/10.1007/s00382-002-0239-7

Dooley, H., Martin, J., & Ellett, D. (1984). Abnormal hydrographic conditions in the Northeast Atlantic during the 1970s. *Rapp PV Reun Cons Int Explor Mer*, *185*, 179–187.

ECCO Consortium, I., Fukumori, Wang, O., Fenty, I., Forget, P., G.and Heimbach, & Ponte, R. M. (n.d.). ECCO Central Estimate (Version 4 Release 4). Retrieved from https://ecco.jpl.nasa.gov/drive/files/version4/release4.

Forget, G., Campin, J.-M., Heimbach, P., Hill, C. N., Ponte, R. M., & Wunsch, C. (2015). ECCO version 4: an integrated framework for non-linear inverse modeling and global ocean state estimation. *Geoscientific Model Development*, *8*(10), 3071–3104. doi: https://doi.org/10.5194/gmd-8-3071-2015

Foukal, N. P., & Lozier, M. S. (2017). Assessing variability in the size and strength of the North Atlantic subpolar gyre. *Journal of Geophysical Research: Oceans*, *122*(8), 6295-6308. doi: https://doi.org/10.1002/2017JC012798

Foukal, N. P., & Lozier, M. S. (2018). Examining the Origins of Ocean Heat Content Variability in the Eastern North Atlantic Subpolar Gyre. *Geophysical Research Letters*, *45*(20), 11,275-11,283. doi: https://doi.org/10.1029/2018GL079122

Fox, A. D., Handmann, P., Schmidt, C., Fraser, N., Rühs, S., Sanchez-Franks, A., ... Yashayaev, I. (2022). Exceptional freshening and cooling in the eastern subpolar North Atlantic caused by reduced Labrador Sea surface heat loss. *Ocean Science*, *18*(5), 1507–1533. doi: https://doi.org/10.5194/os-18-1507-2022

Good, S. A., Martin, M. J., & Rayner, N. A. (2013). EN4: Quality controlled ocean temperature and salinity profiles and monthly objective analyses with uncertainty estimates. *Journal of Geophysical Research: Oceans*, *118*(12), 6704-6716. doi: https://doi.org/10.1002/2013JC009067

Haine, T. W., Siddiqui, A. H., & Jiang, W. (2023). Arctic freshwater impact on the atlantic meridional overturning circulation: status and prospects. *Philosophical Transactions of the Royal Society A*, *381*(2262), 20220185. doi: https://doi.org/10.1098/rsta.2022.0185

Holliday, N. P. (2003). Air-sea interaction and circulation changes in the northeast Atlantic. *Journal of Geophysical Research: Oceans*, *108*(C8). doi: https://doi.org/10.1029/2002JC001344

Holliday, N. P., Bersch, M., Berx, B., Chafik, L., Cunningham, S., Cristian, F.-L., ... Yashayaev, I. (2020). Ocean circulation causes the largest freshening event for 120 years in eastern subpolar North Atlantic. *Nature Communications*, *11*. doi: https://doi.org/10.1038/s41467-020-14474-y

Holliday, N. P., & Cunningham, S. A. (2013). The Extended Ellett Line: Discoveries from 65 Years of Marine Observations West of the UK. *Oceanography*, *26*(2), 156–163.

Hátún, H., Payne, M., Beaugrand, G., Reid, P., Sandø, A., Drange, H., ... Bloch, D. (2009). Large bio-geographical shifts in the north-eastern Atlantic Ocean: From the subpolar gyre, via plankton, to blue whiting and pilot whales. *Progress in Oceanography*, *80*(3), 149-162. doi: https://doi.org/10.1016/j.pocean.2009.03.001

Hátún, H., Sandø, A. B., Drange, H., Hansen, B., & Valdimarsson, H. (2005). Influence of the Atlantic Subpolar Gyre on the Thermohaline circulation. *Science*, *309*(5742), 1841-1844. doi: https://doi.org/10.1126/science.1114777

Häkkinen, S., & Rhines, P. B. (2004). Decline of Subpolar North Atlantic Circulation During the 1990s. *Science*, *304*(5670), 555-559. doi: https://doi.org/10.1126/science.1094917

Häkkinen, S., Rhines, P. B., & Worthen, D. L. (2011). Warm and saline events

embedded in the meridional circulation of the northern North Atlantic. *Journal of Geophysical Research: Oceans*, *116*(C3). doi: https://doi.org/10.1029/2010JC006275

Josey, S. A., & Marsh, R. (2005). Surface freshwater flux variability and recent freshening of the North Atlantic in the eastern subpolar gyre. *Journal of Geophysical Research: Oceans*, *110*(C5). doi: https://doi.org/10.1029/2004JC002521

Joyce, T. M., & Zhang, R. (2010). On the Path of the Gulf Stream and the Atlantic Meridional Overturning Circulation. *Journal of Climate*, *23*(11), 3146 - 3154. doi: https://doi.org/10.1175/2010JCLI3310.1

Koul, V., Tesdal, J.-E., Bersch, M., Hátún, H., Brune, S., Borchert, L., ... Baehr, J. (2020). Unraveling the choice of the north Atlantic subpolar gyre index. *Scientific reports*, *10*(1), 1–12. doi: https://doi.org/10.1038/s41598-020-57790-5

Loose, N., Abernathey, R., Grooms, I., Busecke, J., Guillaumin, A., Yankovsky, E., ... Martin, P. (2022). GCM-Filters: A Python Package for Diffusion-based Spatial Filtering of Gridded Data. *Journal of Open Source Software*, *7*(70), 3947. doi: https://doi.org/10.21105/joss.03947

Medvedev, D., Lemson, G., & Rippin, M. (2016). Sciserver Compute: Bringing Analysis Close to the Data. In *Proceedings of the 28th international conference on scientific and statistical database management.* New York, NY, USA: Association for Computing Machinery. doi: https://doi.org/10.1145/2949689.2949700

Nguyen, A. T., Pillar, H., Ocaña, V., Bigdeli, A., Smith, T. A., & Heimbach, P. (2021). The Arctic Subpolar Gyre sTate Estimate: Description and Assessment of a Data-Constrained, Dynamically Consistent Ocean-Sea Ice Estimate for 2002–2017. *Journal of Advances in Modeling Earth Systems*, *13*(5), e2020MS002398. (e2020MS002398 2020MS002398) doi: https://doi.org/10.1029/2020MS002398

Nye, J. A., Joyce, T. M., Kwon, Y.-O., & Link, J. S. (2011). Silver hake tracks changes in Northwest Atlantic circulation. *Nature communications*, *2*(1), 412. doi: https://doi.org/10.1038/ncomms1420

Oldenburg, D., Armour, K. C., Thompson, L., & Bitz, C. M. (2018). Distinct Mechanisms of Ocean Heat Transport Into the Arctic Under Internal Variability and Climate Change. *Geophysical Research Letters*, *45*(15), 7692-7700. doi: https://doi.org/10.1029/2018GL078719

Piecuch, C. G. (2017). *A note on practical evaluation of budgets in ECCO version 4 release 3* (Tech. Rep.). Retrieved from `http://hdl.handle.net/1721.1/111094`

Piecuch, C. G., Ponte, R. M., Little, C. M., Buckley, M. W., & Fukumori, I. (2017). Mechanisms underlying recent decadal changes in subpolar North Atlantic Ocean heat content. *Journal of Geophysical Research: Oceans*, *122*(9), 7181-7197. doi: https://doi.org/10.1002/2017JC012845

Reverdin, G., Niiler, P. P., & Valdimarsson, H. (2003). North Atlantic Ocean surface currents. *Journal of Geophysical Research: Oceans*, *108*(C1), 2-1-2-21. doi: https://doi.org/10.1029/2001JC001020

Sanchez-Franks, A., & Zhang, R. (2015). Impact of the Atlantic meridional overturning circulation on the decadal variability of the Gulf Stream path and regional chlorophyll and nutrient concentrations. *Geophysical Research Letters*, *42*(22), 9889-9887. doi: https://doi.org/10.1002/2015GL066262

Sanders, R. N. C., Jones, D. C., Josey, S. A., Sinha, B., & Forget, G. (2022). Causes of the 2015 North Atlantic cold anomaly in a global state estimate. *Ocean Science*, *18*(4), 953–978. doi: https://doi.org/10.5194/os-18-953-2022

Sarafanov, A., Falina, A., Sokov, A., & Demidov, A. (2008). Intense warming and salinification of intermediate waters of southern origin in the eastern subpolar North Atlantic in the 1990s to mid-2000s. *Journal of Geophysical Research:*

Oceans, *113*(C12). doi: https://doi.org/10.1029/2008JC004975

Schauer, U., & Losch, M. (2019). "Freshwater" in the Ocean is Not a Useful Parameter in Climate Research. *Journal of Physical Oceanography*, *49*(9), 2309 - 2321. doi: https://doi.org/10.1175/JPO-D-19-0102.1

Sundby, S., & Drinkwater, K. (2007). On the mechanisms behind salinity anomaly signals of the northern North Atlantic. *Progress in Oceanography*, *73*(2), 190 - 202. doi: https://doi.org/10.1016/j.pocean.2007.02.002

Tesdal, J.-E., & Abernathey, R. P. (2021). Drivers of Local Ocean Heat Content Variability in ECCOv4. *Journal of Climate*, *34*(8), 2941 - 2956. doi: https://doi.org/10.1175/JCLI-D-20-0058.1

Tesdal, J.-E., Abernathey, R. P., Goes, J. I., Gordon, A. L., & Haine, T. W. N. (2018). Salinity Trends within the Upper Layers of the Subpolar North Atlantic. *Journal of Climate*, *31*(7), 2675 - 2698. doi: https://doi.org/10.1175/JCLI-D-17-0532.1

Tesdal, J.-E., & Haine, T. W. N. (2020). Dominant Terms in the Freshwater and Heat Budgets of the Subpolar North Atlantic Ocean and Nordic Seas From 1992 to 2015. *Journal of Geophysical Research: Oceans*, *125*(10), e2020JC016435. doi: https://doi.org/10.1029/2020JC016435

Thierry, V., de Boisséson, E., & Mercier, H. (2008). Interannual variability of the Subpolar Mode Water properties over the Reykjanes Ridge during 1990–2006. *Journal of Geophysical Research: Oceans*, *113*(C4). doi: https://doi.org/10.1029/2007JC004443

Weijer, W., Haine, T. W., Siddiqui, A. H., Cheng, W., Veneziani, M., & Kurtakoti, P. (2022). Interactions between the arctic mediterranean and the atlantic meridional overturning circulation: A review. *Oceanography*, *35(3-4)*. doi: https://doi.org/10.5670/oceanog.2022.130

Yan, X., Zhang, R., & Knutson, T. R. (2017). The role of Atlantic overturning circulation in the recent decline of Atlantic major hurricane frequency. *Nature Communications*, *8*(1), 1695. doi: https://doi.org/10.1038/s41467-017-01377-8

Yan, X., Zhang, R., & Knutson, T. R. (2018). Underestimated AMOC Variability and Implications for AMV and Predictability in CMIP Models. *Geophysical Research Letters*, *45*(9), 4319-4328. doi: https://doi.org/10.1029/2018GL077378

Yeager, S. (2015). Topographic Coupling of the Atlantic Overturning and Gyre Circulations. *Journal of Physical Oceanography*, *45*(5), 1258 - 1284. doi: https://doi.org/10.1175/JPO-D-14-0100.1

Yeager, S., Karspeck, A., Danabasoglu, G., Tribbia, J., & Teng, H. (2012). A Decadal Prediction Case Study: Late Twentieth-Century North Atlantic Ocean Heat Content. *Journal of Climate*, *25*(15), 5173 - 5189. doi: https://doi.org/10.1175/JCLI-D-11-00595.1

Zhang, J., Weijer, W., Steele, M., Cheng, W., Verma, T., & Veneziani, M. (2021). Labrador Sea freshening linked to Beaufort Gyre freshwater release. *Nature communications*, *12*(1), 1–8. doi: https://doi.org/10.1038/s41467-021-21470-3

Zhang, R. (2008). Coherent surface-subsurface fingerprint of the Atlantic meridional overturning circulation. *Geophysical Research Letters*, *35*(20). doi: https://doi.org/10.1029/2008GL035463

Zhang, R., & Vallis, G. K. (2006). Impact of Great Salinity Anomalies on the Low-Frequency Variability of the North Atlantic Climate. *Journal of Climate*, *19*(3), 470 - 482. doi: https://doi.org/10.5194/gmd-8-3071-201510.1175/JCLI3623.1